PERIODICA POLYTECHNICA SER. EL. ENG. VOL. 50, NO. 1–2, PP. 103–113 (2006)

INVESTIGATION OF MYOCARDIAL SHORT-SCAN SPECT SCHEMES USING A REAL INHOMOGENEOUS ATTENUATING MEDIUM

Ákos SZLÁVECZ

Department of Control Engineering and Information Technology
Budapest University of Technology and Economics
H–1117 Budapest, Magyar Tudósok krt. 2, Hungary
e-mail: szlavecz@iit.bme.hu

Received: April 28, 2005

Abstract

In myocardial perfusion SPECT imaging the effect of photon attenuation may introduce artifacts in the reconstructed image due to the highly non-uniform distribution of tissue in the thorax region, potentially resulting in false-positive interpretations. It was the general consideration that the adequate compensation of photon attenuation requires, that the emission data be measured at projection angles over 2π in the case the attenuation medium is inhomogeneous. The reduction of the scanning angle in SPECT imaging may be desirable because it can reduce scanning time and thereby minimize patient-motion and other artifacts. In SPECT myocardial imaging emission data is measured historically at projection angles over π from the right anterior oblique (RAO) to the left posterior oblique (LPO). This configuration results in better image contrast and, in some cases, better spatial resolution. However, in this case the reconstructed image may suffer more severely from geometric distortion than 2π angular sampling.

It has been proven recently in analytical computer simulation studies that the data function over 2π in SPECT with non-uniform attenuation contains redundant information; therefore the scanning angle theoretically can be reduced from 2π to π without loss of information.

In this study our goal was to investigate how the various short-scan SPECT scheme configurations work in a real myocardial SPECT imaging system with highly inhomogeneous attenuating medium using attenuation correction. The measured projection images were reconstructed using the Maximum Likelihood Expectation Maximization algorithm with attenuation correction. The reconstructed slices of the various short-scan configurations and the full-scan slices were compared by a cardiac stress/rest software package.

Keywords: myocardial SPECT imaging, attenuation correction, short-scan, pi-scheme.

1. Introduction

Single Photon Emission Computer Tomography (SPECT) is an important nuclear medicine imaging technique that is widely used in myocardial perfusion studies. Several physical effects may affect artifacts in reconstructed images. The most important physical effect is the photon attenuation. Te effect of photon attenuation is particularly disturbing in myocardial perfusion studies due to the highly non-uniform distribution of tissue in the thorax region, potentially resulting in false-positive interpretations [1, 2].

It was the general consideration that the adequate compensation of photon attenuation requires the measurement of the emission data at projection angles over 2π, because in the thorax region the factor photon attenuation is spatially variant, therefore photons in opposite directions suffer different attenuation. Even so in SPECT myocardial perfusion imaging emission data are measured historically at projection angles over π starting from the right anterior oblique (RAO) to the left posterior oblique (LPO), because investigations showed that this configuration results in better image contrast and, in some cases, in better spatial resolution. However, in this case the reconstructed image may suffer from geometric distortion [12, 13].

It has been recently proved that the 2D SPECT images with uniform attenuation over 2π contain redundant information therefore the scanning angle can be reduced from 2π to π [3, 4]. The reduction of the scanning angle in SPECT imaging may be desirable because it can maximize the number of detected photons and improve the signal-to-noise ratio in the emission data. The other advantage of the scan reduction is that it can reduce scanning time and thereby minimize patient-motion and other artifacts.

PAN et al. [5] have developed a heuristic perspective (called 'potato peeler' perspective) to show that the data function over 2π in SPECT with non-uniform attenuation and 3D distance-dependent spatial resolution (3D DDSR) acquired with parallel-beam collimation contains redundant information. They have showed that this redundant information can be used to reduce the scanning angle from 2π to π in SPECT with both non-uniform attenuation and 3D DDSR. PAN et al. conducted analytical computer simulation studies in various pi-scheme scanning configurations [7], and the results corroborated the observations obtained based upon the potato peeler perspective. The pi-scheme convention is defined by Pan in the following way: 'pi-scheme SPECT entails data acquisition over disjoint angular intervals without conjugate views, totaling to π radians' [7].

In this study our goal was to investigate how the short-scan SPECT schemes with various pi-scheme configurations work in a real myocardial SPECT imaging system with highly inhomogeneous attenuating medium using attenuation correction.

2. Methods

2.1. Reconstruction Algorithm: ML-EM with Attenuation Correction

The goal of the reconstruction algorithm used in SPECT is the reconstruction of the distribution of radioactive tracer in the human body based on the projection images. One of the most widely used iterative reconstruction methods for emission tomography is the Maximum Likelihood (ML) Reconstruction using the Expectation Maximization (EM) algorithm [9, 10]. The ML-EM reconstruction is an

iterative solver for a linear system of equations:

$$b = A \cdot x \tag{1}$$

where b is a known vector containing the measured data values, x is the set of image pixels to reconstruct, and A is the transfer matrix containing probability factors between each of the image pixels and each of the measured data values. The transfer matrix coefficient a_{ij} is the probability that a photon emitted in voxel j per unit time is detected in detector location i. This is mathematically expressed by the equation:

$$b_i = \Delta t_i \cdot \sum_{j=1}^{J} x_j \cdot a_{ij} \tag{2}$$

where Δt_i is the imaging time of the i^{th} projection.

There are J different image voxels and I detector locations. The ML-EM estimate for the $(k+1)$-iteration is defined by the equation:

$$x_j^{(k+1)} = x_j^k \frac{1}{\sum_{i=1}^{I} a_{ij}} \sum_{i=1}^{I} \frac{b_i}{\Delta t_i \sum_{n=1}^{J} x_n^k \cdot a_{ni}} \cdot a_{ji} \tag{3}$$

With this method the attenuation can be incorporated into the model by modifying the a_{ij} values in the transfer matrix [11].

The inclusion of attenuation in the transfer matrix requires apriori knowledge of the attenuation map. If the attenuation map is known, the forward problem of the ML-EM algorithm is stated as:

$$b_i = \Delta t_i \cdot \sum_{j=1}^{J} x_j \cdot a_{ij} \cdot e^{-\sum_{n \in N_{ij}} c_{in} \cdot \mu_n} \tag{4}$$

where μ_j is the linear attenuation coefficient of the j^{th} pixel of the attenuation map, and c_{ji} is the effective attenuation length of μ_j. The set N_{ij} is a set of pixels that cover the attenuation line integral from the source pixel j to the projection bin i. This leads to a variation of the ML-EM algorithm with attenuation correction:

$$x_j^{(k+1)} = x_j^k \frac{1}{\sum_{i=1}^{I} a_{ij} \cdot e^{-\sum_{n \in N_{ij}} c_{in} \cdot \mu_n}} \sum_{i=1}^{I} \frac{b_i \cdot e^{-\sum_{n \in N_{ij}} c_{in} \cdot \mu_n}}{\Delta t_i \sum_{n=1}^{J} x_n^k \cdot a_{in} \cdot e^{-\sum_{h \in N_{in}} c_{ih} \cdot \mu_h}} \cdot a_{ij} \tag{5}$$

2.2. Determination of the Attenuation Map

In clinical and research applications adequate methods must be performed to generate the attenuation map. This can be done for example through transmission scanning, segmented MRI data, or appropriately scaled CT scans acquired either independently on separate or simultaneously on multimodality imaging systems. In a clinical environment, the most widely used attenuation correction techniques use transmission data acquired before (preinjection), during (simultaneous), or after (postinjection) the emission scan [6].

In this study we used a sequential scanning method. In this method we measured two kinds of scans: a blank scan and a transmission scans.

The blank scan is made prior to the transmission scans. The blank scan images are generated by measuring the total number of photons transmitted for T_b seconds without the patient.

After the physical phantom is placed into the scanner the transmission scans are recorded for T_t seconds. This gives the transmission image series $T\ (\rho, \theta)$.

Assume that in both scans the number of photons transmitted from the radioactive source in one second to the detector is I_0. Neglecting the absorbtion in air the measured matrix B is given by:

$$B = T_b \cdot I_0 \cdot e^{-\int \mu_{hw} ds} \tag{6}$$

The transmission projection images – with the physical phantom in the scanner – (T) differ from image B by the absorption in the physical phantom:

$$T = T_t \cdot I_0 \cdot e^{-\int \mu_{hw} ds} \cdot e^{-\int \mu_{phantom} ds} \tag{7}$$

The mass attenuation coefficients can be calculated:

$$\mu = -\log\left(\frac{B \cdot T_t}{T \cdot T_b}\right) \tag{8}$$

By reconstructing this image series with the ML-EM algorithm, we obtain the attenuation maps, which can be used for attenuation correction.

2.3. Pi-scheme Configurations

In this work we investigate the reconstruction of so-called pi-scheme SPECT [7] with a real, non-uniform attenuating medium in several pi-scheme configurations. In pi-scheme SPECT the full angular range 2π is divided into angular intervals, and the data are acquired only over disjoint angular intervals whose summation without conjugate views is equal to π. So any pi-scheme scan have data at θ or at $\theta + \pi$. By properly selecting different set of projection angles a various configuration of pi-scheme data can be generated. *Fig. 1* shows the configurations and the sinograms of the four pi-scheme configurations that are applied in this work.

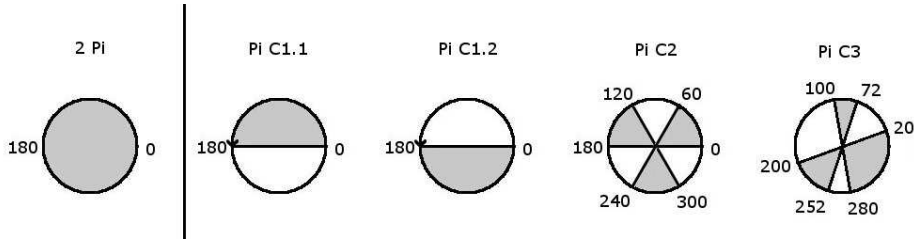

Fig. 1. The various pi-scheme configurations, considered in this work

2.4. Description of Experiments

In the first phase of the research we have conducted a simulation study to test the correctness of our ML-EM algorithm with attenuation correction. Therefore a ring activity distribution is defined with a non-uniform attenuation map showed in *Fig. 2*. The projection image series are generated with the SIMSET Monte Carlo code [8]. The generated images contain 35000-120000 total counts per images depending on the detector angular position. 64 projection images of a 64x64 matrix over a 2π angular view are generated. In this case blank scan and transmission scans were not generated. During the data reconstruction the ideal attenuation maps were used.

In the second phase of the research we used a real myocardial image SPECT system. For data acquisition the Mediso DHV dual head gamma camera were used with LEHR parallel beam collimator, and with a FOV over 530mm $\times$ 390mm: A detailed description of the detector can be found [14].

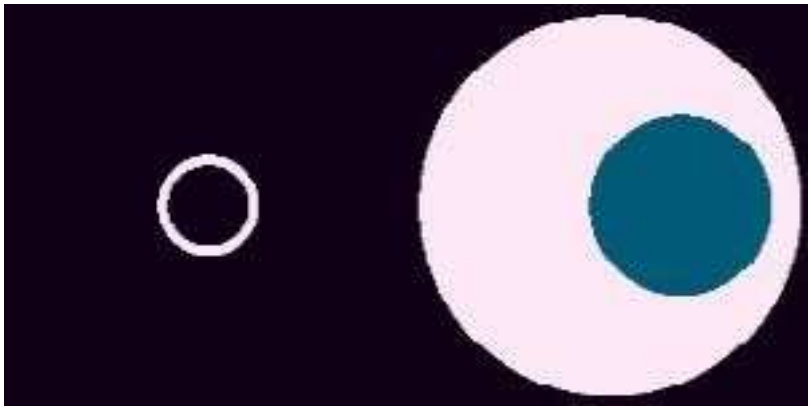

Fig. 2. Simulated activity distribution and attenuation map.

To model the human body we used a standard human torso phantom with cardiac and lung insert extended with a breast phantom. The breasts were modelled by two 0.5 liter infusion bags. As a radionucline tracer Tc-99m were used to model

distribution activity. In the human torso there was injected 75 MBq activity, in the cardiac region 12 MBq activity and in the breasts 4-4 MBq activity of Tc-99m.

There were three steps of the experiments.

In the first step a blank scan image was recorded with the dual head gamma camera. The human torso was removed from the field of view if the gamma camera. A Co57 sheet source was fixed on head 2, and a long time image recording over 1 hour was performed with head 1. This way we get the blank scan image.

In the second step a transmission scan was recorded. The Co57 sheet source was leaved on head 2, and the human torso without the Tc-99m activity distribution was placed in the field of view of the gamma camera. A projection image series of a 64x64 matrix was recorded over pi angular view in 64 steps. Data were aquired for 120 seconds by each image.

In the third step the emission data were aquired. The Co57 sheet source was removed from the field of view of the gamma camera, the human torso, the cardiac insert and the breast phantom was filled with the appropriate Tc-99m activity. Finally an emission projection image series of 64x64 matrix was recorded over a 2π angular view in128 steps. The starting angle was the right anterior oblique. By each image was aquired data for 60 seconds.

3. Results

The simulated images and the images of the human torso were reconstructed with the ML-EM reconstruction algorithm with attenuation correction described above. After the reconstruction the images obtained by using full scan images are compared by the images obtained by using pi-scheme (ie. partial scan) images.

At first a visual check was performed, then the reconstructed slices of the various pi-scheme configurations and the full-scan slices were re-oriented and compared by using the cardiac stress/rest software package (called InterView) of Mediso Ltd [15]. During the comparisons the base image series was always the reconstructed full-scan image series, which is called in the result figures as ‘stress’ according to the naming convention of stress/rest software package. The compared image series – obtained by the various pi-scheme configurations – is called as ‘rest’.

Fig. 3 and *Fig. 4* show the sinograms and the appropriate reconstructed slice of the simulated ring activity object in the following order (from left to right): full-scan, pi-scheme C1.1, pi-scheme C1.2, pi-scheme C2, pi-scheme C3. The reconstructed slices of the various pi-scheme configurations seem to be identical with the reconstructed full-scan slice. The slice pi-scheme C1.1 and C3 seem to be a little bit more inhomogeneous in the activity region than the full-scan slice.

The result of the comparison obtained by the cardiac stress/rest software package is shown in *Fig 5* and *Fig 6*. The curves are almost identical which corresponds to the case of identical images. The structures of the activity regions of the pi-scheme configurations (described by the curves in *Fig. 5* and *Fig. 6*) and the activity regions of the full-scan image are very similar to each other.

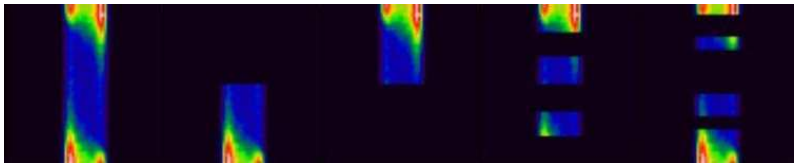

Fig. 3. Sinograms of the simulation of the various configurations. From left to right: full-scan, pi-Scheme C1.1, pi-scheme C1.2, pi-scheme C2, pi-scheme C3

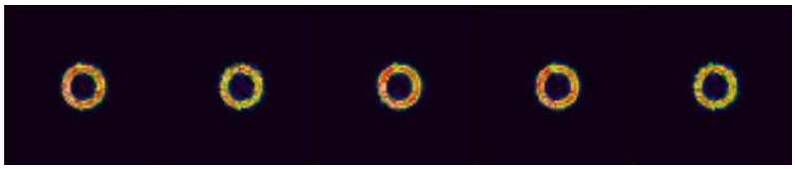

Fig. 4. Reconstructed slices of the simulation. From left to right: full-scan, pi-scheme C1.1, pi-scheme C1.2, pi-scheme C2, pi-scheme C3

Fig. 7 shows the appropriate attenuation map sinogram and the reconstructed attenuation map. *Fig. 8* and *Fig. 9* show the sinograms and the appropriate reconstructed slice of the human torso phantom in the following order (from left to right): full-scan, pi-scheme C1.1, pi-scheme C1.2, pi-scheme C2, pi-scheme C3. For the illustration we used the slice number 37 out of the 64 slices.

In the sinogram of the pi-scheme configuration C1.1 (the scanning angle range from 180 to 360 was used) the structure of the cardiac region cannot be easily recognized by visual check, the signal to noise ratio is too low. In this angle range the emitted photons go through a medium with bigger attenuation factor. This is the reason of the weaker quality of this reconstruction. This disturbance can be recognized on the reconstructed slice too, compare the second slice from left on *Fig. 9* with the other slices.

After the manual comparison of the reconstruction the comparison by cardiac stress/rest software was performed. The result of the comparison can be seen on *Fig 10* and *Fig. 11*. The curves of the pi-scheme configurations C1.2, C2 and C3 are almost identical to the full-scan configuration. The structures of the activity regions are again very similar to each other.

In the case of the configuration C1.1 a decreased activity can be seen in septal direction. Probably the imperfect statistical characteristics (i.e. the signal to noise ratio is to low) of the projection images in the angle range 180-360 can cause this effect. Note that during the reconstruction we did not apply distance-dependent spatial resolution correction. PAN et al. in they analytical study have not reported similar effects [5].

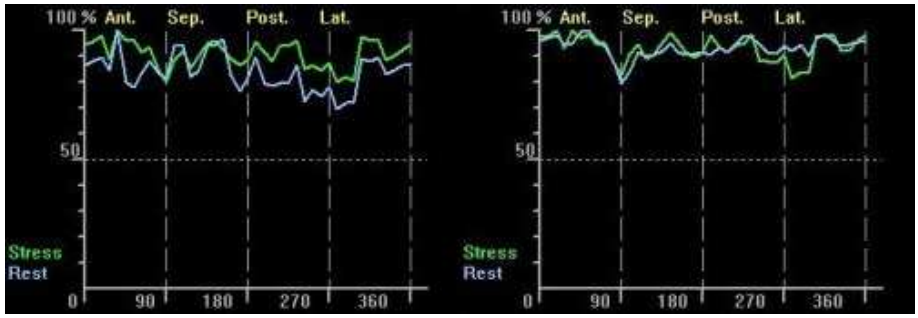

Fig. 5. Reoriented and compared reconstructed image series of the simulation. The curves represent normalized line integral values in axial direction after the reorientation. Pi-scheme C1.1 on the left, pi-scheme C1.2 on the right

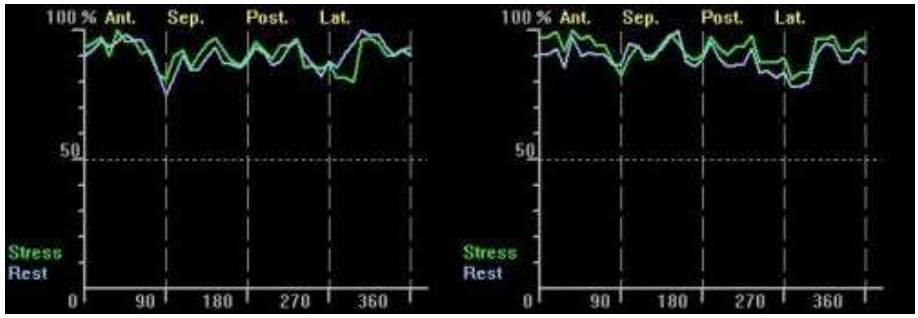

Fig. 6. Reoriented and compared reconstructed image series of the simulation. The curves represent normalized line integral values in axial direction after the reorientation. Pi-scheme C2 on the left, pi-scheme C3 on the right

4. Conclusion

In this study our goal was to investigate how the short-scan SPECT schemes with various pi-scheme configurations work in a real myocardial SPECT imaging system with highly inhomogeneous attenuating medium using attenuation correction.

After data acquisition we reconstructed the measured projection images using the ML-EM algorithm with attenuation correction. The reconstructed slices of the various pi-scheme configurations and the full-scan slices were re-oriented and compared.

In the comparison we found in the pi-scheme configuration C1.1 (in this configuration the scanning angle range from LPO to RAO was used) a decreased image quality in septal direction, probably caused by a low signal to noise ratio.

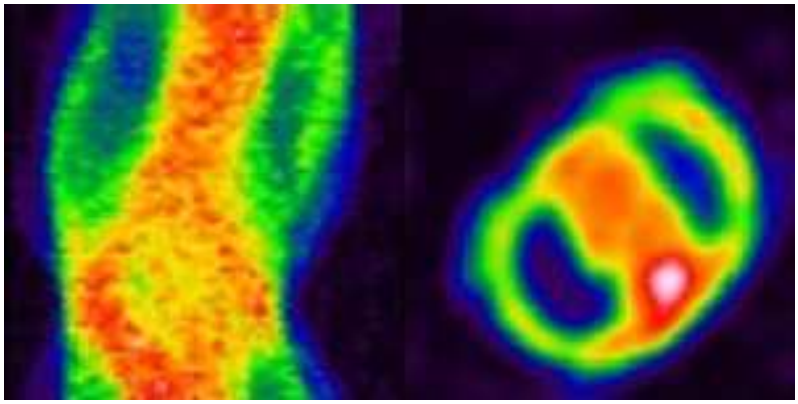

Fig. 7. The sinogram and the reconstructed attenuation map of slice 37

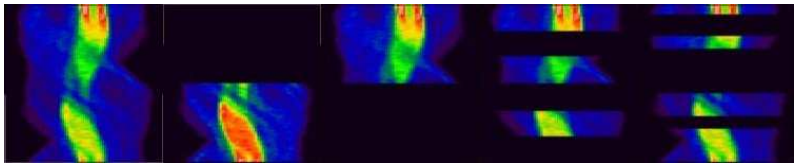

Fig. 8. Sinograms of the human torso phantom of slice 37 in various configurations. From left to right: full-scan, pi-Scheme C1.1, pi-scheme C1.2, pi-scheme C2, pi-scheme C3

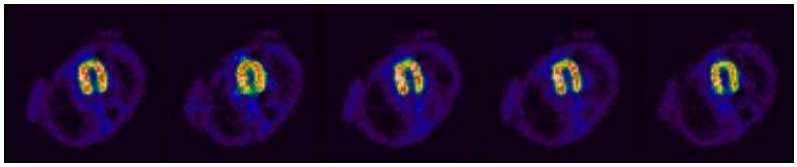

Fig. 9. Reconstructed slices of the human torso phantom of slice 37 in various configurations. From left to right: full-scan, pi-scheme C1.1, pi-scheme C1.2, pi-scheme C2, pi-scheme C3.

The other pi-scheme configurations investigated in this study are comparable to the full-scan slices.

By these results we proved that the scanning angle reduction can be applied in real myocardial SPECT imaging systems. This result correlates to the clinical practice where the de-facto standard configuration in SPECT myocardial perfusion imaging is the π angle range from RAO to LPO.

Based on our results we can state that there are many more other pi-scheme

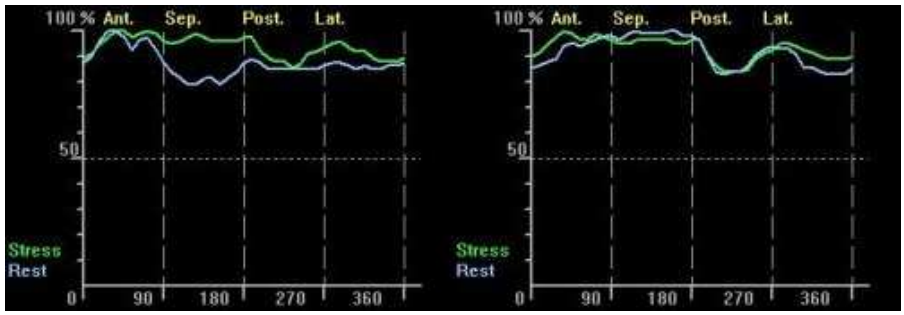

Fig. 10. Reoriented and compared reconstructed image series of the human torso phantom. The curves represent normalized line integral values in axial direction after the reorientation. Pi-Scheme C1.1 on the left, pi-scheme C1.2 on the right.

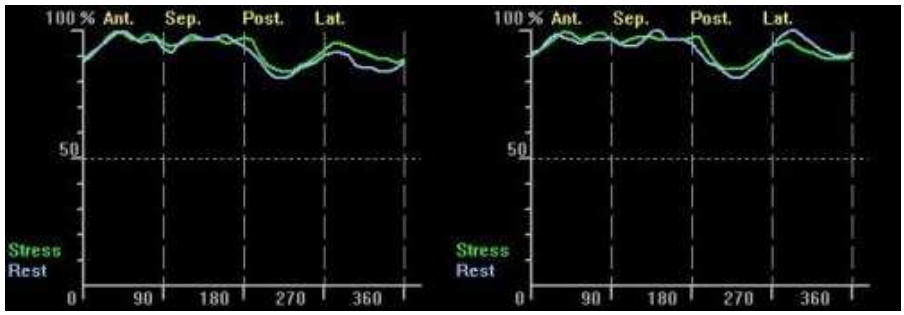

Fig. 11. Reoriented and compared reconstructed image series of the human torso phantom. The curves represent normalized line integral values in axial direction after the reorientation. Pi-scheme C2 on the left, pi-scheme C3 on the right.

configurations that can result in good-quality image reconstruction comparable to the full-scan slices.

A question for the future is, which pi-scheme configuration is optimal for using in practice. It is a possible solution to select the optimal set of projection angles in a pi-scheme scanning configuration based on the signal to noise ratio. The clarification of this question is the object of our further work.

Acknowledgement

This research work was supported by Mediso Ltd and by the Hungarian National Research Found, Grants No. OTKA F046726, T042990. The author wishes to thank dr. Tamás Bükki and Balázs Benyó for their helpful assistance.

References

[1] HENDEL, R.–CORBETT, J.–CULLOM, S.–DEPUEY, E.–GARCIA, E.–BATEMAN, T., The Value and Practice of Attenuation Correction for Myocardial Perfusion SPECT Imaging: A Joint Position Statement from the American Society of Nuclear Cardiology and the Society of Nuclear Medicine, *J. Nucl. Med.*, **43** (2002), pp. 273–280.

[2] WACKERS, F., Attenuation correction, or the emperor's new clothes?, *J. Nucl. Med.*, **40** (1999), pp. 1310–1312.

[3] METZ, C. E.–PAN, X., A Unified Analysis of Exact Methods of Inverting the 2-D Exponential Radon Transform, with Implications for Noise Control in SPECT, *IEEE Trans. Med. Imaging,* **14** (1995), pp. 643–58.

[4] NOO, F.–WAGNER, J-M., Image Reconstruction in 2D SPECT with 180-degree Acquisition, *Inverse Problems*, **17** (2001)**,** pp. 1357–72.

[5] PAN, X.–SIDKY, E.Y.–KAO, C. M.-ZOU, Y.–METZ, C. E., Short-scan SPECT imaging with Non-uniform Attenuation and 3D Distance-dependent Spatial Resolution, *Phys. Med. Biol.*, **47** (2002), pp. 2811-2833.

[6] ZAIDI, H.-HASEGAWA, B., Determination of the Attenuation Map in Emission Tomography, *J. Nucl. Med.*, **44/2** (2003), pp. 291–315.

[7] PAN, X.-KAO, C-M.–SIDKY, E.Y.–ZOU, Y.–METZ, C.E., Pi-Scheme Short-Scan SPECT and Image Reconstruction With Nonuniform Attenuation, *IEEE Trans. Nucl. Science*, **50/1** (2003), pp. 87–96.

[8] HARRISON, R.L.–HAYNOR, D.R.–GILLISPIE, S.B.–VANNOY, S. D.–KAPLAN, M. S.–LEWELLEN, T. K., A Public-domain Simulation System for Emission Tomography Photon Tracking through Heterogeneous Attenuation Using Importance Sampling, *J. Nucl. Med.*, **34/5** (1993), p. 60.

[9] LANGE, K.–CARSON, R., EM Reconstruction Algorithm for Emission and Transmission Tomography, *Journal of Computer Assisted Tomography*, **8/2** (1984), pp. 306–316.

[10] SHEPP, L.A.–VARDI Y., Maximum Likelihood Reconstruction for Emission Tomography, *IEEE Trans. Med. Imaging*, **1** (1982), pp. 113-122.

[11] HAWKINS, W. G., Source-assisted Attenuation Correction for Emission Computer Tomography, United States Patent, Patent No. US 6,339,652 B1, Jan. 15. 2002.

[12] KNESAUREK, K. – KING, M. A. – GLICK, S. J. – PENNEY, B. C., Investigation of Causes of Geometric Distortion in 180° and 360° angular sampling in SPECT, *J. Nucl. Med.*, **30** (1989), p. 1666.

[13] GO, R. T. – MACINTYRE, W. J. – HOUSER, T. S. – PANTOJA, M. – O DONNEL, J. K. – FEIGLIN, D. H. – SUFKA, B. J. – UNDERWOOD, D. A.– MEANEY, T. F., Clinical Evaluation of 360° and 180° Data Sampling Techniques for Transaxial SPECT Thallium-201 Mycardial Perfusion Imaging, *J. Nucl. Med.*, **26** (1985), p. 695.

[14] Description of the Dual-head Gamma Camera, Mediso Ltd.: http://www.mediso.com/products/universal-line/spirit-dh-v/overview.html

[15] InterView, the Nuclear Medical Image processing Software Package, Mediso Ltd.: http://www.mediso.hu